

Realization of Hz-Level Rabi Spectra in Shallow Optical Lattice Clock

Mo-Juan Yin,^{1,2,*} Tao Wang,^{3,4,*} Xiao-Tong Lu,¹ Ting Li,^{1,2}
Jing-Jing Xia,¹ Xue-Feng Zhang,^{3,4,†} and Hong Chang^{1,2,‡}

¹Key Laboratory of Time and Frequency Primary Standards,

National Time Service Center, Chinese Academy of Sciences, Xi'an 710600, China

²School of Astronomy and Space Science, University of Chinese Academy of Sciences, Beijing 100049, China

³Department of Physics, and Center of Quantum Materials and Devices,
Chongqing University, Chongqing, 401331, China

⁴Chongqing Key Laboratory for Strongly Coupled Physics, Chongqing, 401331, China

The quantum metrology with ultra-high precision usually requires the atoms prepared in an ultra-stable environment with well-defined quantum states. Thus, the optical lattice clock system chooses deep lattice potential to trap the ultra-cold atoms. However, building atomic clock in shallow optical lattice can greatly reduce decoherence rate induced by Raman scattering as well as higher order light shift, but tunneling among the lattice sites will cause additional dephasing and strongly broadening of the Rabi spectrum. Here, we periodically drive the shallow ^{87}Sr optical lattice clock in the experiment. Counterintuitively, shaking the system can deform the wide broad spectral line into a sharp peak with 5.4Hz line-width. With careful comparison between the theory and experiment, we demonstrate the Rabi frequency and Bloch bands can be simultaneously and independently tuned by adjusting the driving frequency and amplitude. Our work not only provides a different idea for quantum metrology, such as building shallow optical lattice clock in outer space, but also paves the way for quantum simulation of new phase of matter, such as engineering exotic spin orbit coupling Hamiltonian.

Introduction.- Spectroscopy is a fundamental exploratory tool in various fields, including physics, chemistry, astronomy and so on. The line-width of the spectral line directly determines the frequency sensitivity to systematic noise, and will be broadened by the local and non-local effects. As one of the most accurate time frequency measurement devices and candidate for the next standard of time [1–4], the optical lattice clock (OLC) system utilizes the ultra-narrow spectral line provided by the interacting between the ultra-narrow line-width laser and the two-level ultra-cold ^{87}Sr atoms. In order to weaken the broadening caused by inter-site tunneling process, the atoms are trapped in a deep optical lattice potential [5–7]. However, the strong trapping potential can introduce higher order light shifts [8] and enhance the decoherence caused by Raman scattering [9]. Thus, depressing the inter-site tunneling becomes one of the central tasks for the shallow OLC. The straightforward strategies are using gravity potential difference to break translational symmetry[8] or increasing the lattice constant [10], but as a smoking gun, the ultra-narrow spectral line in shallow OLC has never been observed.

The quantum tunneling process is easier for lower potential barrier, so the shallow optical lattice with weak inter-site tunneling is counterintuitive. However, as the conventional approach of the Floquet engineering (FE), periodically shaking lattice can modify the Bloch-band structure and even suppress the tunneling between nearest-neighbor sites completely [11–13]. Therefore, considering no obvious heating problem and extra noise are observed in previous implementation of FE in OLC platform [14, 15], the FE turns out to be ideal solution for realization of ultra-narrow spectral line in shallow OLC

system. Then, two major advantages are immediately brought out. It is naturally suitable for the environment without gravity, such as in spaceship or satellite [16]. Meanwhile, it could be easily extended to different geometry, such as three dimensional OLC system [7].

In this manuscript, we report a Hz-level spectrum experimentally observed in a shallow OLC system. In order to suppress the inter-site tunneling of ultra-cold atoms, we design a Floquet engineering method implemented on the lattice laser with triangle periodical frequency modulation. As shown in Fig.1 (a-b), a wide spectral line with low excitation fraction is observed for undriven case. In comparison, a sharp spectral line with 5.4Hz line-width can be clearly observed when the lattice potential is periodically driven. Based on the Floquet theory, we find the Bloch bands can be tuned via changing the driving amplitude, and the effective Rabi frequency is related to the ratio between driving amplitude and frequency. It indicates both of them can be independently adjusted. The modulation function of Rabi frequency is experimental verified in deep lattice. Meanwhile, after preparing the atoms at different Bloch bands in the shallow lattice, the modulation function of hopping amplitude is also checked in the experiment. Finally, we try to further lower the lattice potential and test the limitation of our approach.

Experiment setup.- We trapped an ensemble of nuclear spin-polarized ($m_F = +9/2$) two level ^{87}Sr atoms in a quasi-one dimensional optical lattice formed by two counter-propagating lasers which originated from unequally splitting one lattice laser at a ‘magic’ wavelength of $\lambda_L = 813.4\text{nm}$. As shown in Fig.1 (c), both of them are tunable with the help of AOM. The stronger one provides a global energy shift which is equivalent to a

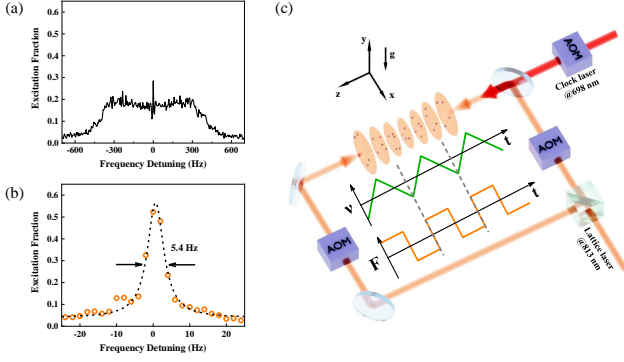


Figure 1. The Rabi spectra of population in excited state at $U_z = 9.1E_r$, $g_0 = 21\text{Hz}$ with probe time $t = 150\text{ms}$. (a) In the undriven case, the spectrum is weak and broad ($\sim\text{kHz}$). (b) In the driven case with driving amplitude $\nu_a = 13.7644\text{kHz}$ and frequency $\nu_s = 600\text{Hz}$, a strong and narrow spectral line emerges with 5.4Hz line-width estimated by Lorentz function fitting (dash line). (c) Experimental setup: The ^{87}Sr atoms are trapped in one dimensional optical lattice formed with two counter-propagating lattice laser beams which can be tuned via the acousto-optic modulator (AOM). Differently, the frequency of the stronger lattice laser is locked to the magic wave length, and the Floquet engineering is implemented on the weaker one. Meanwhile, the AOM attached to the clock laser is used for band preparation and measurement. The inset presents the effective triangle periodical velocity $v(t)$ of atoms and effective force $F(t)$ they feel.

system-size flat potential [17], so that about 10^4 atoms can be trapped at low temperature ($\sim 3\mu\text{K}$), but this flat potential is not necessary for a three dimensional OLC system [7]. The amplitude and frequency of the weak lattice laser can be changed by voltage variable attenuator (VVA) and AOM [15]. After interacting with the clock laser at a wavelength of $\lambda_p = 698\text{nm}$, the atoms at the ground state ($5s^2\ ^1S_0(|g\rangle)$) will be excited to higher energy level ($5s5p\ ^3P_0(|e\rangle)$) which has a long life time ($\sim 160\text{s}$). When tuning the frequency of the clock laser, the measurement of the population in the excited state P_e can provide the Rabi spectra (see supplementary material [18] for details).

As the ingredient of Floquet engineering, the frequency of the weak lattice laser is periodically driven following with triangle signal function:

$$\Delta\nu(t) = \begin{cases} \nu_a \left(\frac{4t}{T_s} - 1 \right) & 0 \leq t < T_s/2 \\ \nu_a \left(3 - \frac{4t}{T_s} \right) & T_s/2 \leq t < T_s \end{cases} \quad (1)$$

in which ν_a is the driving amplitude, $T_s = 1/\nu_s$ is the period with the driving frequency ν_s . In the experiments, we set ν_a less than 20kHz and ν_s ranging from several hundred to several kilo Herz, so the influence of deviation from ‘magic’ wavelength can be neglected [14]. As shown in the inset of Fig.1 (c), the periodic driven makes

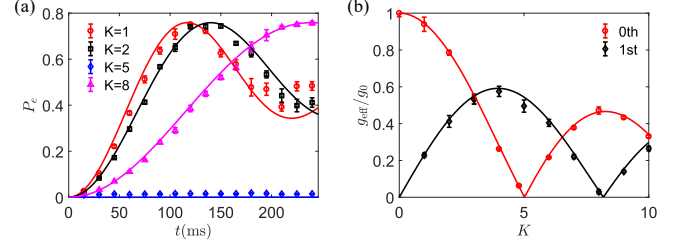


Figure 2. (a) The Rabi oscillation of the zeroth Floquet sideband at different renormalized driving amplitude K . The dot lines are experiment data, and the solid lines are theoretical results with same fitting parameters [14]. (b) The ratio between effective Rabi frequency of the zeroth and first order Floquet sidebands and the bare one g_{eff}/g_0 vs the renormalized driving amplitude K (dots line). The effective Rabi frequency is extracted from the experiment measurement of corresponding Rabi oscillation. Meanwhile, the solid lines are the modulation function $\mathcal{R}^m(K)$.

the atoms feel an effective velocity $v(t) = \lambda_L \Delta\nu(t)/2$ with triangle form, and additional effective force $F(t) = \frac{M\lambda_L}{2} \frac{d\Delta\nu(t)}{dt}$ with square form in which M is the mass of ^{87}Sr atoms. Then based on the Floquet theory (see supplementary material [18] for details), it is found that the Rabi frequency and Bloch bands can be engineered independently and simultaneously. In order to verify it, we first perform our experiments in deep lattice with depth $U_z = 90E_r$ ($E_r = \frac{\hbar^2 k_L^2}{2M} \approx 3.44\text{kHz} \times \hbar$, which is the recoil energy).

Engineering of Rabi frequency.- When the lattice potential is much strong, the system could be approximately taken as two level atoms in identical harmonic traps. Then, the Bloch bands barely contribute to the Rabi spectrum, so that the influence of driving on the Rabi frequency can be singled out. Because the bare Rabi frequency g_0 is much smaller than ν_s , we can use the resolved side-band approximation [14]. Then, the carrier band will split into numbers of Floquet sidebands, and the effective Rabi frequency of m th Floquet sideband is $g_{\text{eff}}^m = g_0 \mathcal{R}^m(K)$. The modulation function can be explicitly represented as

$$\mathcal{R}^m(K) = \int_{-\frac{1}{2}}^{\frac{1}{2}} \cos(m\pi t) \cos\left(\frac{\Phi K}{2}\left(t^2 - \frac{1}{4}\right) + \frac{m\pi}{2}\right) dt \quad (2)$$

in which $K = \nu_a/\nu_s$ is the renormalized driving amplitude and the phase $\Phi = \pi\lambda_L/\lambda_p \approx 7\pi/6$ is related to the spin orbit coupling (SOC) induced by incommensurate ratio between wavelengths of lattice and clock lasers [17]. Different from conventional Bessel function form [11], the Eq.(2) contains the Fresnel integrals [18].

In order to extract the effective Rabi frequency, we measure the Rabi oscillation at different renormalized driving amplitudes. As demonstration of Fig.2 (a), the driven strongly changes the population of excitation. Especially at $K = 5$, the excitation is even smaller than

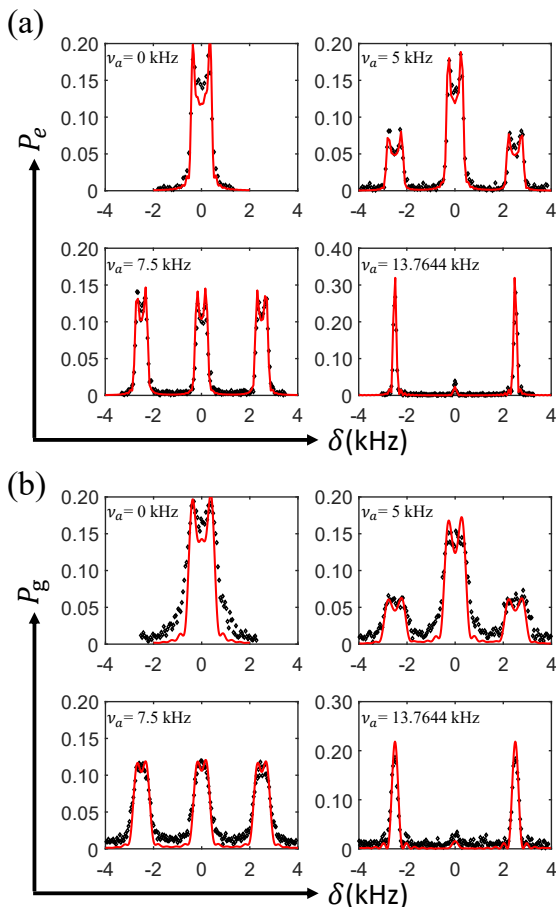


Figure 3. (a) The Rabi spectrum of the atoms prepared at the internal state $|g\rangle$ of $n_z = 0$ Bloch band. The experimental parameters are $U_z = 9E_r$, $g_0 = 104\text{Hz}$, the probe time $t = 6\text{ms}$, and the driving frequency is fixed at $\nu_s = 2.5\text{kHz}$. (b) The Rabi spectrum of the atoms prepared at the internal state $|e\rangle$ of $n_z = 1$ Bloch band. The experimental parameters are $U_z = 27.2E_r$, $g_0 = 196.7\text{Hz}$, the probe time $t = 3\text{ms}$, and the driving frequency is fixed at $\nu_s = 2.5\text{kHz}$. The fitting parameters of theoretical results (red solid lines) are identical as the undriven case.

the noise background, and it indicates the effective Rabi frequency is nearly zero. Actually, it is much close to the zero point of $\mathcal{R}^0(K)$ which is $K = 5.023$. After extracting g_{eff}^m and dividing it by g_0 , the measurement of modulation function can be obtained. Same as the Rabi oscillation, the experiment results matches well with the theoretical result in Fig.2 (b), and the curves of both zeroth and first order Floquet sideband follow the modulation function $\mathcal{R}^m(K)$. The suppressing point $K = 8$ of first order Floquet sideband is also consistent with the theoretical prediction $K = 8.18$.

Engineering of Bloch bands.- When the lattice potential becomes shallow, the inter-site tunneling of the ultracold atoms can not be ignored. The hopping amplitude between l th and l' th sites $J_{l,l'}^{\vec{n}}$ ($\vec{n} = (n_x, n_y, n_z)$) can be calculated in harmonic basis (n_x, n_y) in transverse direc-

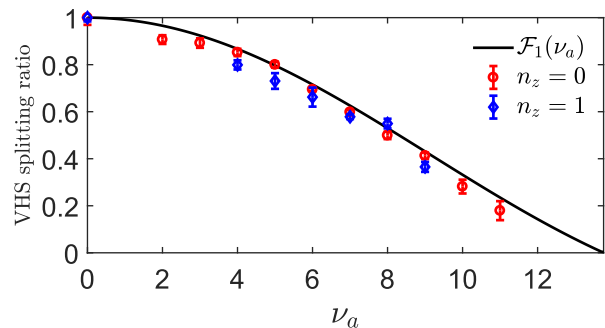


Figure 4. The VHS splitting ratio with driving amplitude ν_a for both $n_z = 1$ and $n_z = 0$, which is in consistent with modification function $\mathcal{F}_1(\nu_a)$.

tions and Wannier basis n_z in longitude direction. Then, the system can be described by a quantum many body Hamiltonian [18]. When shaking the lattice, all atoms at different \vec{n} states feel the same effective force, so all the hopping processes are modulated simultaneously. When the driving frequency is much larger than system parameters, but still much smaller than the band gap, there is no 'Floquet photon assisted hopping' between different bands. Then the hopping amplitudes of all states are dressed by following normalized sinc function

$$\mathcal{F}_{l-l'}(\nu_a) = \text{sinc}\left(\frac{\hbar\nu_a}{4E_r}|l-l'|\right), \quad (3)$$

with \hbar the Plank constant. It is quite unusual that the modulation function of bands $\mathcal{F}_{l-l'}(\nu_a)$ only depends on ν_a , while $\mathcal{R}^m(K)$ is the function of the renormalized driving amplitude K . Meanwhile, the other relevant parameters Φ , \hbar and E_r are constants in the experiment. It indicates both modulations can be independently tuned by only changing ν_a and ν_s , which is important for not only Floquet engineering [13] but also the quantum simulation [19].

The atoms in the shallow lattice approximately follow the Boltzmann distribution on the Bloch bands labeled with index (q, \vec{n}) where q is the momentum. In order to verify the Eq.3, we prepare all the atoms at $n_z = 0$ and $n_z = 1$ separately, so the dephasing effect between them can be avoided. In the experiment, the atoms are loaded into a deep shaken lattice potential ($U_z = 90E_r$) with target driving amplitude and frequency. Then, after energy filtering and adiabatic decreasing lattice potential to $9E_r$ in 100ms , nearly all the atoms are prepared at the internal state $|g\rangle$ of $n_z = 0$ th Bloch band [18]. The Fig.3 (a) shows the Rabi spectrum at a π pulse interrogation and driving frequency $\nu_s = 2.5\text{kHz}$ for different driving amplitudes ν_a . In the undriven case, the carrier peak is broadened and split to the line shape with double peaks, which are typical features of Van Hove singularity (VHS) due to SOC [17]. When turning on the drive, the Floquet sidebands appear with VHS splitting line-shape.

However, the VHS splitting width decreases during enhancing the driving amplitude. Until $\nu_a = 13.7644\text{kHz}$ which is closed to zero point solution $\nu_a^0 = 4E_r/h$ of Eq.3, the carrier peak is almost suppressed accompanying with two high 1st Floquet sidebands which do not exhibit VHS splitting. The height variation of the Floquet sidebands can be understood from the modulation of the Rabi frequency. When $\nu_a = 13.7644\text{kHz}$, the renormalized driving amplitudes $K = \nu_a/\nu_s \approx 5.5$ is quite close to the zero point of $\mathcal{R}^0(K)$, so the excitation rate is very weak at zero detuning. On the other hand, considering the nearest neighbor hopping in the tight-banding approximation [17], the explicit expression of the VHS band splitting width is

$$W_{n_z}(\nu_a) = 8\langle J_1^{\vec{n}} \rangle_{T_r} \mathcal{F}_1(\nu_a) \sin(\Phi/2), \quad (4)$$

in which $\langle J_1^{\vec{n}} \rangle_{T_r}$ represents the thermal average of the hopping according to the transverse temperature T_r . It is clear finding that the VHS splitting width is irrelevant to the Floquet number and monotonically decreases while increasing ν_a to ν_a^0 .

Different from band preparation of $n_z = 0$, the target lattice depth for $n_z = 1$ Bloch bands is chosen to be deeper $U_z = 27.25E_r$, because it can trap more atoms while keeping the hopping amplitude close to $n_z = 0$. Besides that, the atoms are prepared in the internal excited state $|e\rangle$, so the Rabi spectrum is according to the population of the ground state P_g . As shown in Fig.3 (b), a similar phenomenon can be observed, which indicates that hopping amplitude of different bands are modulated simultaneously, as predicted by our theory. In order to quantitatively verify the modulation factor of the Bloch bands, we extract the VHS splitting width by taking the positions of the VHS peaks. After divided by the undriven width, the VHS splitting width ratios are plotted in Fig.4. It is clear that both $n_z = 1$ and $n_z = 0$ data matches well with the theoretical prediction $W_{n_z}(\nu_a)/W_{n_z}(0) = \mathcal{F}_1(\nu_a)$. Thus, we experimentally demonstrate the Bloch bands are simultaneously modulated with the same modulation function, and it indicates we do not need to prepare the system at even lower temperature to suppress the hopping, which will cause severe atom loss.

Narrow Rabi spectrum.- Last but not least, we experimentally realized the Hz-level spectral line. The driving amplitude is set to be $\nu_a = 13.7644\text{kHz}$, so that the hopping amplitude can be suppressed by a factor of 10^{-6} . Indeed, from the modulation function $\mathcal{F}_{l-\nu}(\nu_a)$, we can clearly find it not limited to the nearest neighbor, all the inter-site hopping will be simultaneously suppressed to zero while ν_a approaching to ν_a^0 . That is why the triangle form periodical driving is chosen instead of the conventional sinusoidal type. Although the next nearest neighbor hopping is much smaller than the nearest neighbor one, the VHS splitting is still tens of Hz for $n_z = 1$ when the lattice potential goes down to $15E_r$. Furthermore,

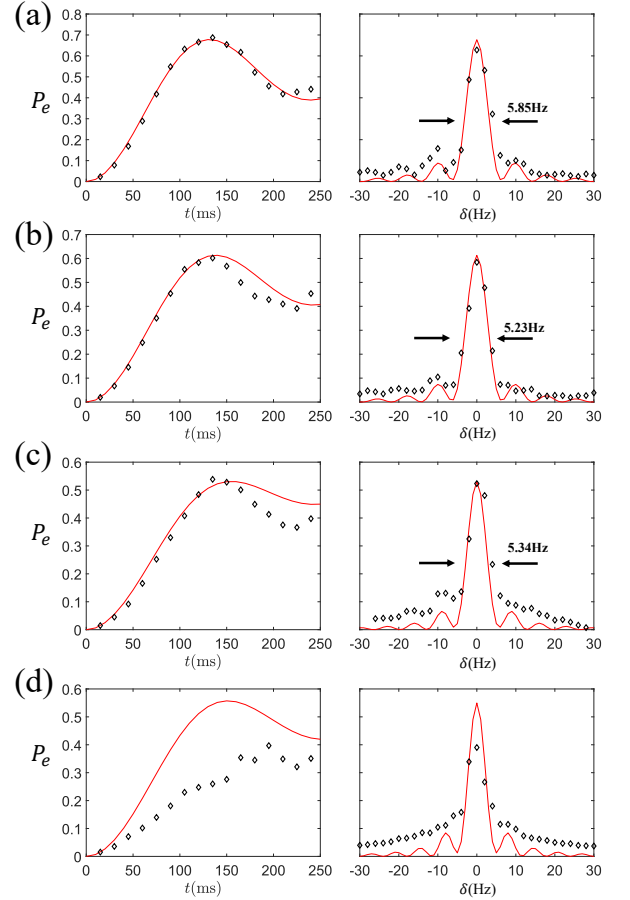


Figure 5. The experiment data of Rabi oscillations (left) and spectra (right) are measured at driving amplitude $\nu_a = 13.7644\text{kHz}$, driving frequency $\nu_s = 600\text{Hz}$ and bare Rabi frequency $g_0 = 21\text{Hz}$ with different lattice potentials and probe times ((a) $U_z = 23E_r$, $t = 135\text{ms}$, (b) $U_z = 15.1E_r$, $t = 135\text{ms}$, (c) $U_z = 9.1E_r$, $t = 150\text{ms}$ and (d) $U_z = 7.2E_r$, $t = 150\text{ms}$). The theoretical results of Rabi oscillations (left) and Rabi spectrum (right) are red solid lines. The FWHM of carrier peaks in (a), (b) and (c) are obtained by Lorentz function fitting. The FWHM for $U_z = 7.2E_r$ is not given, because its spectral line is not of Lorentz type.

due to the long interrogation time, ν_s should be small to avoid driving caused heating problem. Meanwhile, it should be much larger than the system parameter so that the effective Hamiltonian obtained from high frequency expansion theory is still valid. Thus, we set the driving frequency as $\nu_s = 600\text{Hz}$ in our experiment.

The experiment data of Rabi oscillation and spectrum after a π pulse clock laser interrogation for optical lattice potential with various depths are presented in Fig.5. The Rabi oscillation matches well with the theoretical prediction even at very shallow lattice $U_z = 9.1E_r$. Because the ν_a and ν_r are not changed, the renormalized driving amplitude K is the same for different lattice potential. Most importantly, the Hz-level ($\sim 5\text{Hz}$) Rabi spectra has a high signal-to-noise ratio, and their full width at half

maxima (FWHM) is close to the Fourier limit. The consistency of both the Rabi oscillation and the spectrum data between theory and experiment indicates that the driven under this condition does not bring serious noise or heating problem despite long interrogation time.

Certainly, such Floquet engineering still has its limitations. As demonstrated in Fig.5 (d), when the lattice potential goes down to $7.2E_r$, the experimental data starts to deviate from the theoretical prediction. The effective Rabi frequency is apparently much smaller, and meanwhile the Rabi spectrum can not keep its line-shape as Lorentz form. Such limitation may result from the atoms hopping between different Bloch bands with the help of “Floquet photons”, and improvement requires exploration of more complicated Floquet engineering approaches in the future.

Conclusion and Outlook.- The ultra-stable periodical modulation method is developed for independently Floquet engineering the Rabi frequency and the Bloch bands, so that the Hz-level Rabi spectrum can be realized in a shallow OLC system. This work paves the way for building atomic clock in a shallow optical lattice. It can not only reduce the dephasing caused by large lattice potential, but also be easy to generate to higher dimensional OLC. Different from the conventional method using gravity potential difference to suppress the hopping, our method does not depend on gravity, so it might be useful for atomic clock systems operated in space. On the other hand, our work also benefits quantum simulation in OLC, e.g. one could combine FE and even-odd site symmetry breaking to change the SOC phase Φ or design a more complex form of driven to simulate exotic Hamiltonian. Further attractive direction will be quantitative analysis of heating or photon assisted hopping, based on the high precision of OLC.

This work is supported by the National Natural Science Foundation of China (Grant No. 61775220), the Key Research Project of Frontier Science of the Chinese Academy of Sciences (Grant No. QYZDB-SSW-JSC004) and the Strategic Priority Research Program of the Chinese Academy of Sciences (Grant No. XDB35010202). T. W. is supported by the Special Foundation for Theoretical Physics Research Program of China (Grant No. 11647165) and the China Postdoctoral Science Foundation Funded Project (Project No. 2020M673118). X.-F. Z. acknowledges funding from the National Science Foundation of China under Grants No. 11804034, No. 11874094 and No.12047564, Fundamental Research Funds for the Central Universities Grant No. 2020CDJQY-Z003 and 2021CDJZYJH-003.

* These authors contributed equally to this work.

† zhangxf@cqu.edu.cn

‡ changhong@ntsc.ac.cn

- [1] M. Takamoto and H. Katori, Phys. Rev. Lett. **91**, 223001 (2003).
- [2] J. Ye, H. J. Kimble, and H. Katori, Science **320**, 1734 (2008).
- [3] A. D. Ludlow, M. M. Boyd, J. Ye, E. Peik, and P. O. Schmidt, Rev. Mod. Phys. **87**, 637 (2015).
- [4] Boulder Atomic Clock Optical Network Bacon Collaboration, K. Beloy, M. I. Bodine, T. Bothwell, S. M. Brewer, S. L. Bromley, J.-S. Chen, J.-D. Deschênes, S. A. Diddams, R. J. Fasano, T. M. Fortier, Y. S. Hassan, D. B. Hume, D. Kedar, C. J. Kennedy, I. Khader, A. Koepke, D. R. Leibrandt, H. Leopardi, A. D. Ludlow, W. F. McGrew, W. R. Milner, N. R. Newbury, D. Nicolodi, E. Oelker, T. E. Parker, J. M. Robinson, S. Romisch, S. A. Schäffer, J. A. Sherman, L. C. Sinclair, L. Sonderhouse, W. C. Swann, J. Yao, J. Ye, and X. Zhang, Nature (London) **591**, 564 (2021).
- [5] S. Blatt, J. W. Thomsen, G. K. Campbell, A. D. Ludlow, M. D. Swallows, M. J. Martin, M. M. Boyd, and J. Ye, Phys. Rev. A **80**, 052703 (2009).
- [6] B. J. Bloom, T. L. Nicholson, J. R. Williams, S. L. Campbell, M. Bishof, X. Zhang, W. Zhang, S. L. Bromley, and J. Ye, Nature (London) **506**, 71 (2014), arXiv:1309.1137 [physics.atom-ph].
- [7] S. L. Campbell, R. B. Hutson, G. E. Marti, A. Goban, N. Darkwah Oppong, R. L. McNally, L. Sonderhouse, J. M. Robinson, W. Zhang, B. J. Bloom, and J. Ye, Science **358**, 90 (2017).
- [8] P. Lemonde and P. Wolf, Phys. Rev. A **72**, 033409 (2005).
- [9] M. Bishof, M. J. Martin, M. D. Swallows, C. Benko, Y. Lin, G. Quéméner, A. M. Rey, and J. Ye, Phys. Rev. A **84**, 052716 (2011), arXiv:1108.1431 [physics.atom-ph].
- [10] R. B. Hutson, A. Goban, G. E. Marti, L. Sonderhouse, C. Sanner, and J. Ye, Phys. Rev. Lett. **123**, 123401 (2019).
- [11] A. Eckardt, C. Weiss, and M. Holthaus, Phys. Rev. Lett. **95**, 260404 (2005).
- [12] H. Lignier, C. Sias, D. Ciampini, Y. Singh, A. Zenesini, O. Morsch, and E. Arimondo, Phys. Rev. Lett. **99**, 220403 (2007).
- [13] A. Eckardt, Rev. Mod. Phys. **89**, 011004 (2017).
- [14] M.-J. Yin, T. Wang, X.-T. Lu, T. Li, Y.-B. Wang, X.-F. Zhang, W.-D. Li, A. Smerzi, and H. Chang, Chin. Phys. Lett. **38**, 073201 (2021).
- [15] X.-T. Lu, T. Wang, T. Li, C.-H. Zhou, M.-J. Yin, Y.-B. Wang, X.-F. Zhang, and H. Chang, Phys. Rev. Lett. **127**, 033601 (2021).
- [16] S. Origlia, M. S. Prasad, S. Schiller, Y. Singh, K. Bongs, R. Schwarz, A. Al-Masoudi, S. Dörscher, S. Herbers, S. Häfner, U. Sterr, and C. Lisdat, Phys. Rev. A **98**, 053443 (2018).
- [17] S. Kolkowitz, S. L. Bromley, T. Bothwell, M. L. Wall, G. E. Marti, A. P. Koller, X. Zhang, A. M. Rey, and J. Ye, Nature (London) **542**, 66 (2017), arXiv:1608.03854 [cond-mat.quant-gas].
- [18] See Supplemental Material at <http://link.aps.org/supplemental/xxx> for a discussion of further details about experimental realizations, Floquet theory and Band preparation.
- [19] F. Schäfer, T. Fukuhara, S. Sugawa, Y. Takasu, and Y. Takahashi, Nature Reviews Physics **2**, 411 (2020), arXiv:2006.06120 [cond-mat.quant-gas].

SUPPLEMENT MATERIALS

Experimental Setup

The atoms are cooled down to about $3\mu\text{K}$ by two-stage Doppler cooling, and then loaded into a quasi-one-dimensional lattice formed by overlapping two counter-propagating lattice laser beams produced by splitting one lattice laser with beam waist about $W_0 \approx 60\mu\text{m}$. The stronger laser beam fixes its power to $P_1 = 600\text{mW}$, and the power of weaker one P_2 can be tuned from 0.7 to 185mW, so that the lattice potential can change from near 0 to $90E_r$. The frequency of each beam can be independently adjusted by acousto-optic modulator (AOM), and the power of tunable lattice beam can be changed by controlling the radio frequency signal power of AOM by a variable voltage attenuator (VVA). The radio frequency signal is offered by an arbitrary function generator (AFG, Tektronix AFG3252C), so that the triangle function modulation can be added to modulate the lattice laser frequency. The clock laser (made by STABLE LASER SYSTEM. co) is stabilized to a 10-cm-long ultra-low-expansion cavity and its line-width is about 1 Hz. The clock laser beam is overlapped with the lattice and its polarization is along the direction of the gravity, and the same as both lattice beams. The preparation of atoms in the Bloch bands can be found in the supplementary materials.

Model and Floquet Theory

In the experiment, the lattice potential of the interfered counter-propagating laser beams can be clearly written as

$$U(t) = -\frac{U_z}{2} \cos\left(2k_L z - \pi \int_0^t \Delta\nu(\tau) d\tau\right) + \frac{2U_r r^2}{W_0^2} - \eta \frac{2U_r r^2}{W_0^2} \sin^2(k_L z),$$

$$U_z = 4\alpha \frac{\sqrt{P_1 P_2}}{\pi \epsilon_0 c W_0^2}, \quad U_r = \alpha \frac{(\sqrt{P_1} + \sqrt{P_2})^2}{\pi \epsilon_0 c W_0^2}, \quad (5)$$

in which α is the polarizability at the magic wavelength, $\eta = U_z/U_r$ is the coupling constant, ϵ_0 is permittivity of free space, c is the speed of light, and $r = \sqrt{x^2 + y^2}$ represents the position of the atoms perpendicular to the lattice direction z .

In the r direction, we choose the harmonic eigen basis $|n_x, n_y\rangle$ with eigen-energy $(n_x + n_y + 1)h\nu_r$ in which the transverse frequency is $\nu_r = \sqrt{\frac{U_r}{M\pi^2 W_0^2}}$. Meanwhile, in the co-moving frame in z direction, the atoms could be

described as

$$\hat{H}_z(t) = \frac{\hat{p}_z^2}{2M} - \frac{U_z}{2} \cos(2k_L z) - F(t)z, \quad (6)$$

with the effective force $F(t) = \frac{M\lambda_L}{2} \frac{d\Delta\nu(t)}{dt}$. Then the states can be represented in the Wannier basis $|n_z, l\rangle = w_{n_z}(z-l)$ in z direction. Thus, the whole time-dependent Hamiltonian is written as

$$\hat{H}(t) = \hat{H}_z(t) + \hat{H}_r + \hat{H}_c + \hat{H}_{\text{int}}(t). \quad (7)$$

The hopping of atoms under the effective force $F(t)$ in z direction is described by

$$\hat{H}_z = - \sum_{\bar{n}, \sigma} \sum_{l \neq l'} J_{|l-l'|}^{n_z} \left[\hat{c}_{\bar{n}, \sigma, l}^\dagger \hat{c}_{\bar{n}, \sigma, l'} + h.c. \right] - F(t) \sum_{\bar{n}, \sigma, l} l \hat{c}_{\bar{n}, \sigma, l}^\dagger \hat{c}_{\bar{n}, \sigma, l}, \quad (8)$$

where $\hat{c}(\hat{c}^\dagger)$ is the annihilation(creation) operator of the fermion, $\sigma = e, g$ labels the internal states and the hopping amplitude is

$$J_{|l-l'|}^{n_z} = \langle n_z, l | \frac{\hat{p}_z^2}{2Mc} - \frac{U_z}{2} \cos(2k_L z) | n_z, l \rangle. \quad (9)$$

Meanwhile,

$$\hat{H}_r = \sum_{\bar{n}, \sigma, l} h\nu_r (n_x + n_y + 1) \hat{c}_{\bar{n}, \sigma, l}^\dagger \hat{c}_{\bar{n}, \sigma, l} \quad (10)$$

reflects the external states in r direction. The coupling between z and r direction is written as

$$\hat{H}_c = - \sum_{\bar{n}, \sigma} \sum_{l \neq l'} C_{|l-l'|}^{\bar{n}} \left[\hat{c}_{\bar{n}, \sigma, l}^\dagger \hat{c}_{\bar{n}, \sigma, l'} + h.c. \right], \quad (11)$$

where the coupling strength is

$$C_{|l-l'|}^{\bar{n}} = \eta h\nu_r (n_x + n_y + 1) \langle n_z, l | \sin^2(k_L z) | n_z, l \rangle. \quad (12)$$

The last term denotes the interaction between clock laser and the ultra-cold atoms:

$$\hat{H}_{\text{int}} = \sum_{\bar{n}, l} \left[\frac{h(\delta - \frac{v(t)\nu_p}{c})}{2} \left(\hat{c}_{\bar{n}, e, l}^\dagger \hat{c}_{\bar{n}, e, l} - \hat{c}_{\bar{n}, g, l}^\dagger \hat{c}_{\bar{n}, g, l} \right) + \frac{g_{\bar{n}}}{2} (e^{i\Phi} \hat{c}_{\bar{n}, e, l}^\dagger \hat{c}_{\bar{n}, g, l} + h.c.) \right], \quad (13)$$

where δ is the detuning frequency, ν_p is the frequency of clock laser, $v(t) = \lambda_L \Delta\nu(t)/2$ is the velocity of atoms, $\Phi = \lambda_L/\lambda_p \approx 7\pi/6$ denotes the spin orbit coupling effect and the Rabi frequency is $g_{\bar{n}} = g_0 \langle \bar{n}, 0 | e^{i\vec{k}_p \cdot \vec{r}} | \bar{n}, 0 \rangle$.

After implementing two following unitary operators

$$\hat{U}_1 = \exp \left[\frac{i}{\hbar} F(t) \sum_{\bar{n}, \sigma, l} l \hat{c}_{\bar{n}, \sigma, l}^\dagger \hat{c}_{\bar{n}, \sigma, l} \right]$$

$$\hat{U}_2 = \exp \left[\frac{iv(t)\nu_p}{\pi c} \sum_{\bar{n}, l} \left(\hat{c}_{\bar{n}, e, l}^\dagger \hat{c}_{\bar{n}, e, l} - \hat{c}_{\bar{n}, g, l}^\dagger \hat{c}_{\bar{n}, g, l} \right) + i2\pi m\nu_s t \right]$$

on the Hamiltonian 7, the rotating Hamiltonian $\hat{H}_R(t) = \hat{U}_1^\dagger \hat{U}_2^\dagger (\hat{H} - i\hbar \frac{\partial}{\partial t}) \hat{U}_1 \hat{U}_2$ is of the same period T_s . Considering the inter-site hopping amplitudes and the bare Rabi frequency g_0 are much smaller than the driving energy $h\nu_s$ in our experiment, we can calculate the effective time-independent Hamiltonian $\hat{H}_{\text{eff}} = \frac{1}{T_s} \int_0^{T_s} \hat{H}_R(t)$ perturbatively by using Floquet Magnus expansion theory. Then, it can be explicitly written as

$$\begin{aligned} \hat{H}_{\text{eff}} &= \hat{H}_t + \hat{H}_I \quad (14) \\ \hat{H}_t &= - \sum_{\vec{n}, \sigma} \sum_{l \neq l'} J_{|l-l'|}^{\vec{n}} \mathcal{F}_{l-l'}(\nu_a) \left[\hat{c}_{\vec{n}, \sigma, l}^\dagger \hat{c}_{\vec{n}, \sigma, l'} + h.c. \right] + \hat{H}_r \\ \hat{H}_I &= \sum_{\vec{n}, l, m} \left[\frac{h(\delta - m\nu_s)}{2} \left(\hat{c}_{\vec{n}, e, l}^\dagger \hat{c}_{\vec{n}, e, l} - \hat{c}_{\vec{n}, g, l}^\dagger \hat{c}_{\vec{n}, g, l} \right) \right. \\ &\quad \left. + \frac{g_{\vec{n}} \mathcal{R}^m(K)}{2} \left(e^{i l \Phi} \hat{c}_{\vec{n}, e, l}^\dagger \hat{c}_{\vec{n}, g, l} + h.c. \right) \right], \end{aligned}$$

in which $J_{|l-l'|}^{\vec{n}} = J_{|l-l'|}^{n_z} + C_{|l-l'|}^{\vec{n}}$ denotes the hopping between sites l and l' and m denotes the Floquet sideband index. The concise form of $\mathcal{F}_{l-l'}(\nu_a)$ and $\mathcal{R}^m(K)$ could be found in main text, and $\mathcal{R}^m(K)$ could be further integrated as:

$$\begin{aligned} \mathcal{R}^m(K) &= \frac{\pi}{\sqrt{K\Phi}} \left[\cos \left[\frac{(K\Phi - 2m\pi)^2}{8K\Phi} \right] \left(\text{FC} \left[\frac{K\Phi - 2m\pi}{2\sqrt{K\pi\Phi}} \right] \right) \right. \\ &\quad \left. + \text{FC} \left[\frac{K\Phi + 2m\pi}{2\sqrt{K\pi\Phi}} \right] \right) + \sin \left[\frac{(K\Phi - 2m\pi)^2}{8K\Phi} \right] \\ &\quad \left(\text{FS} \left[\frac{K\Phi - 2m\pi}{2\sqrt{K\pi\Phi}} \right] + \text{FS} \left[\frac{K\Phi + 2m\pi}{2\sqrt{K\pi\Phi}} \right] \right) \right], \quad (15) \end{aligned}$$

in which FC and FS are two kinds of Fresnel integrals.

The Hamiltonian above can be exactly solved in the momentum space, and the first term is diagonal with band structure as $E_{|\vec{n}, q\rangle} = -2J_{|l-l'|}^{\vec{n}} \mathcal{F}_{l-l'}(\nu_a) \cos(q) + h\nu_r(n_x + n_y + 1)$ when only considering the nearest neighbor hopping. Then, the internal Hamiltonian \hat{H}_I can be rewritten as

$$\begin{aligned} \hat{H}_I &= \sum_{\vec{n}, q, m} \left[\frac{h(\delta - m\nu_s)}{2} \left(\hat{c}_{\vec{n}, e, q}^\dagger \hat{c}_{\vec{n}, e, q} - \hat{c}_{\vec{n}, g, q}^\dagger \hat{c}_{\vec{n}, g, q} \right) \right. \\ &\quad \left. + \frac{g_{\vec{n}} \mathcal{R}^m(K)}{2} \left(\hat{c}_{\vec{n}, e, q+\Phi}^\dagger \hat{c}_{\vec{n}, g, q} + h.c. \right) \right], \quad (16) \end{aligned}$$

which can be taken as numbers of two-level atoms oscillating between state $|\vec{n}, q\rangle$ and $|\vec{n}, q + \Phi\rangle$ in every Floquet sideband. Thus, the Rabi spectrum of population in state

$|\sigma\rangle$ could be written as

$$P_\sigma(t) = \sum_{\vec{n}, q, m} B(\vec{n}, q) \left| \frac{g_{\text{eff}}^{\vec{n}, m}}{\Omega_\sigma^m} \right|^2 \sin^2(\Omega_\sigma^m \pi t) \quad (17)$$

$$\Omega_e^m = \sqrt{((\delta - m\nu_s) + E_{|\vec{n}, q+\Phi\rangle} - E_{|\vec{n}, q\rangle})^2 + (g_{\text{eff}}^{\vec{n}, m})^2}$$

$\Omega_g^m = \sqrt{((\delta - m\nu_s) + E_{|\vec{n}, q+\Phi\rangle} - E_{|\vec{n}, q\rangle})^2 + (g_{\text{eff}}^{\vec{n}, m})^2}$, in which $B(\vec{n}, q)$ is the Boltzmann distribution factor in states $|\vec{n}, q\rangle$ and $g_{\text{eff}}^{\vec{n}, m} = g_{\vec{n}} \mathcal{R}^m(K)$ is the effective Rabi frequency for m th Floquet band. When only considering the nearest neighbor hopping, the energy difference is $E_{|\vec{n}, q+\Phi\rangle} - E_{|\vec{n}, q\rangle} = 4J_1^{\vec{n}} \mathcal{F}_1(\nu_a) \sin(\Phi/2) \sin(\Phi/2 + q)$, and it indicates the VHS band splitting of different state is $8J_1^{\vec{n}} \mathcal{F}_1(\nu_a) \sin(\Phi/2)$ and irrelevant with the Floquet sideband index m . Last, we got the VHS band splitting is presented as

$$W_{n_z}(\nu_a) = 8 \langle J_1^{\vec{n}} \rangle_{T_r} \mathcal{F}_1(\nu_a) \sin(\Phi/2). \quad (18)$$

Band Preparation

The atoms are first loaded into a deep lattice trap potential with $P_1 = 600\text{mW}$ and $P_2 = 185\text{mW}$ (corresponding to a trap depth of about $90E_r$). Then, the atoms are nuclear spin-polarized to $mF = +9/2$ state by 15-ms-long 689nm pulse. After that, the power of the strong lattice laser beam linearly reduces to $P_1' = 140\text{mW}$ within 20ms, keeps 10ms and linearly raises to 600mW within 15ms. After this process of energy filtering, the remaining atoms almost populates in the Bloch state of $n_z = 0$.

To prepare atoms in the Bloch state of $n_z = 1$, a 100ms long clock laser pulse, of which the frequency corresponds to the maximum excitation fraction of the blue sideband, is used to excite the transition after energy filtering. Then, a 2ms long 461nm pulse is used to clear all remaining atoms. The longitudinal trap frequency ($\nu_z = 64.4(1)\text{kHz}$), longitudinal temperature ($T_z = 1.4\mu\text{K}$), radial atomic temperature ($T_r = 3.1\mu\text{K}$), the number of longitudinal and radial Bloch state ($N_z = 4$ and $N_r \approx 1071$, respectively) are extracted from the resolved sideband spectrum as shown in Fig. S1. After preparing the atoms in expected Bloch state, the power of the other lattice beam (P_2) linearly decreases to P_2' within 20ms to adjust the tunnelling rate.

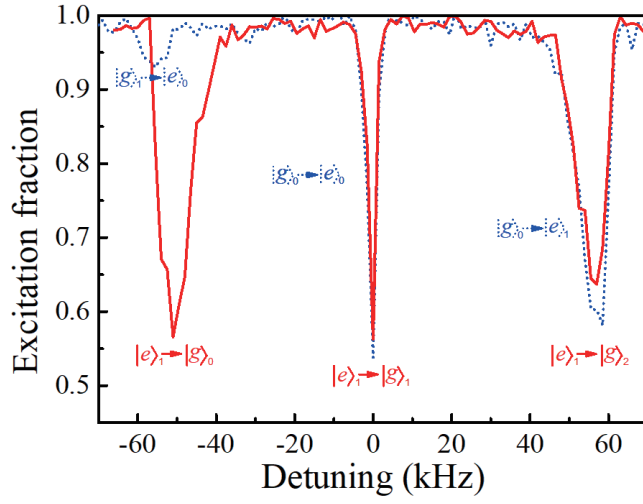


Figure S1. The resolved sideband spectrum in deep lattice without modulation. The blue dash line indicates that the initial state of atoms is prepared into the Bloch state $n_z = 0$. The blue dash line indicates that the initial state of atoms is prepared into the Bloch state $n_z = 1$.